RESEARCH ARTICLE

Comparing wavelet and Fourier perspectives on the decomposition of meridional energy transport into synoptic and planetary components

Tuomas Heiskanen[1] | Rune Grand Graversen[1,2] | Johanne Hope Rydsaa[1] | Pål Erik Isachsen[3,4]

[1]Department of Physics and Technology, University of Tromsø, Tromsø, Norway

[2]Norwegian Meteorological Institute, Tromsø, Norway

[3]Department of Geosciences, University of Oslo, Oslo, Norway

[4]Norwegian Meteorological Institute, Oslo, Norway

Correspondence
T.I.H. Heiskanen, Department of Physics and Technology, University of Tromsø, Postboks 6050, Langnes, 9037 Tromsø, Norway.
Email: tuomas.i.heiskanen@uit.no

Funding information
Research Council of Norway (NFR), Grant/Award Number: 280727

Abstract

The Arctic region shows some of the world's most significant signs of climate change; for instance, a negative trend in summer sea-ice cover of around 15% per decade and Arctic amplified surface-air warming that is three times the global average. The atmospheric energy transport plays an important role in the Arctic climate. Recently a Fourier-based method for studying the atmospheric energy transport contribution by planetary- and synoptic-scale waves has been proposed. Recent studies based on this method show that planetary waves contribute more than synoptic waves to the atmospheric energy transport into the Arctic. However, this Fourier method suffers from being incapable of resolving spatially localized systems such as cyclones. Here an attempt to evaluate this problem is presented by applying the method on synthetic and reanalysis data. In addition, an alternative method based on a wavelet decomposition is proposed and compared with the Fourier-based method. The wavelet method is based on localized basis functions which should be capable of resolving these localized systems. The wavelet method shows an impact of synoptic-scale transport on Arctic temperatures which is not captured by the Fourier method, whilst the planetary-scale effect of both methods appears similar.

KEYWORDS

Arctic amplification, energy transport, latent heat, planetary waves, synoptic waves, wave decomposition, wavelets

1 | INTRODUCTION

The latitudinal variation of incoming solar radiation induces a poleward energy transport in the climate system (Holton and Hakim, 2013). The atmosphere contributes the largest portion of this transport into the Arctic, whilst the ocean contribution is small north of 45°N (Trenberth and Caron, 2001). At the Arctic boundary (∼70°N) the atmospheric contribution is comparable to the incoming solar radiation received by the Arctic (Peixoto and Oort, 1992).

Several atmospheric processes accomplish the meridional energy transport. At low latitudes the Hadley cell is the main contributor, whilst at mid to high latitudes

eddies contribute the major part (Vallis, 2017). The eddies include both planetary-scale Rossby waves ($\gtrsim$ 4,000km) and synoptic-scale cyclones ($\lesssim$ 4,000km), both of which induce meridional energy transport. The atmospheric energy transport is traditionally decomposed into latent heat and dry-static components, and into contributions of transient and stationary eddies (Peixoto and Oort, 1992). The decomposition into stationary and transient eddies does not reveal the structure and spatial scale of the eddies transporting energy, since both planetary- and synoptic-scale systems can be either stationary or transient.

Identifying the contributions of planetary- and synoptic-scale systems to the meridional energy transport is important in order to estimate, for example, the interannual variability of the transport and the effects of climate change on the transport, since these types of waves may respond differently to climate change (Graversen and Burtu, 2016; Yoshimori *et al.*, Nov 2017; Naakka *et al.*, 2019). In order to examine the scale dependency of atmospheric energy transport, a Fourier decomposition method (FDM) used to decompose energy transport into contributions from planetary- and synoptic-scale waves was recently proposed by Graversen and Burtu (2016) hereafter referred to as GB16. Based on the FDM it was shown that planetary-scale waves contribute the largest portion of the atmospheric energy transport at the Arctic boundary and hence contribute more to Arctic warming than do synoptic-scale waves. These findings hold for both the latent heat and dry-static energy transports. By applying the FDM to data from the EC-Earth climate model, it was found that changes in the atmospheric circulation patterns may contribute to the Arctic amplification, even if the overall energy transport remains constant or declines. This is because the Arctic cooling due to a projected reduction of total energy transport encountered due to a decline of the dry-static part will be more than compensated for by the warming caused by the increase in planetary latent heat transport (Koenigk *et al.*, 2013; Graversen and Burtu, 2016).

Several recent studies highlight the importance of synoptic-scale systems for the latent heat transport into the Arctic (Boisvert *et al.*, 2016; Woods and Caballero, 2016; Messori *et al.*, 2018). It is intriguing that the synoptic-scale transport appears to show little influence on Arctic temperatures according to the FDM (Graversen and Burtu, 2016), since other studies show that synoptic-scale systems are important for the latent heat transport into the Arctic. Here we speculate that this discrepancy could be partly due to a misrepresentation of synoptic systems by the FDM.

A Fourier decomposition separates fields into a series of sinusoidal waves. However atmospheric fields are of course seldom composed of pure sinusoidal waves; for example there may exist both sharp zonal gradients and isolated systems simultaneously at one latitude. Such localized systems are not well represented by the FDM, since the Fourier basis is composed of non-localized functions.

This problem can be approached by applying a wavelet decomposition. Wavelets are localized both in space- and length-scale, and are thus capable of representing spatially localized properties of fields. As the basis functions of a wavelet expansion are localized both in length-scale and space, the wavelet method likely represents the spatially localized systems more accurately than the FDM does.

The main objective of this study is to re-evaluate the FDM proposed in GB16 and thus the applicability of Fourier series for zonal wave decomposition of atmospheric fields. The FDM is first evaluated by applying the method on synthetic data where only pure synoptic or pure planetary systems are present. Then the method is applied on filtered fields from the ERA-Interim reanalysis, where the filters are designed to find atmospheric states characterized by isolated cyclones and situations where only planetary waves are present. The same analysis is done using a wavelet decomposition method (WDM) for comparison. Finally both methods are used to assess the effect of latent heat transport on Arctic daily temperatures as in GB16.

The data and methods are presented in Section 2, the results and comparisons in Section 3, and a summary and concluding remarks are provided in Section 4.

2 | DATA AND METHODS

2.1 | Synthetic cyclones

The performance of the FDM and WDM in capturing isolated synoptic-scale systems is first illustrated by applying the methods on synthetic data. The synthetic data are generated to mimic the geopotential height field associated with a longitudinal cross-section through a cyclone centre. The synthetic data are produced with Gaussian functions in the geopotential height field. This approach is applied to ensure that no planetary wave activity is present in the fields used to test the FDM. The winds of the synthetic cyclones are computed assuming geostrophic balance, which is a reasonable assumption in the extratropics (Vallis, 2017).

2.2 | Fourier decomposition method

The FDM approach of GB16 is based on a Fourier series expansion in the zonal direction of the energy field E and

mass transport $v \, \mathrm{d}p/g$, where v is the meridional velocity, p pressure and g is gravitational acceleration. In the present study, only the latent heat transport is considered such that $E = Lq$, where L is the latent heat of evaporation and q is the specific humidity. Here only the final form of the FDM is presented. For the detailed derivation of the FDM the reader is referred to GB16.

A split into wavenumbers by the FDM of the meridional energy transport is given as

$$vE = d \sum_{i=1}^{L} \left\{ \frac{a_{0,i}^v a_{0,i}^E}{4} + \frac{1}{2} \sum_{n=1}^{\infty} \left(a_{n,i}^v a_{n,i}^E + b_{n,i}^v b_{n,i}^E \right) \right\}, \quad (1)$$

where $d = 2\pi r \cos(\phi)$ is the circumference at latitude ϕ, n the wavenumber, L the number of vertical levels in the dataset, r Earth's radius, ϕ the latitude, and a_n and b_n are the Fourier coefficients of $v \, \mathrm{d}p/g$ and E, with wavenumber n at vertical level i. The meridional energy transport in Equation (1) is further decomposed into contributions from the zonal-mean circulation (the first term) and from planetary- and synoptic-scale waves by splitting the last sum of Equation (1) in terms of wavenumbers. In GB16 the planetary waves correspond to wavenumbers 1–5 and synoptic waves to wavenumbers 6–20. The separation between planetary and synoptic waves between wavenumbers 5 ($\sim 2,700$ km at 70°N) and 6 ($\sim 2,280$ km at 70°N) is somewhat arbitrary. In the present study the wavenumber separation between planetary- and synoptic-scale waves is set to between wavenumbers 3 ($\sim 4,500$ km at 70°N) and 4 ($\sim 3,400$ km at 70°N). This is chosen to better match the actual length-scale of synoptic and planetary systems at 70°N of approximately 4,000 km (Holton and Hakim, 2013).

The data used in the present study are the same as used in GB16 for years 1979–2012, and updated by the same method for years 2013–2017. The present study is based on latent heat transport only, which has been shown to affect the Arctic the most (Graversen and Burtu, 2016). The same evaluation as presented here is also applicable for the dry-static energy transport, and is expected to yield similar results.

2.3 | Wavelet decomposition method

An alternative method to the FDM is a wavelet decomposition method (WDM). The WDM developed here is based on a set of basis functions known as wavelets. The WDM is comparable to the Fourier-based FDM in that both methods decompose the meridional energy (ME) transport into components of different length-scales. However there is a difference in the decompositions: whereas the FDM decomposes the ME transport into contributions based on

wavenumbers, n, the WDM performs a decomposition into spatial scales, j. These are not directly comparable, and the relation between wavenumber n from the FDM and scale j from the WDM is dependent on the chosen wavelet.

A function $\psi(x)$ is a wavelet if it has zero mean (Equation (2)) and unit energy (Equation (3)):

$$\int_0^d \psi(x) \, \mathrm{d}x = 0, \quad (2)$$

$$\int_0^d |\psi(x)|^2 \, \mathrm{d}x = 1, \quad (3)$$

where x is the coordinate along a latitude circle with circuit $d = 2\pi r \cos(\phi)$, as for the FDM. From a wavelet, $\psi(x)$, an orthonormal basis is formed by stretching and translation of the wavelet. Additionally, an amplitude scaling is introduced to ensure unit energy of the wavelets (Daubechies, 1992). The orthonormal basis can be shown to be

$$\psi_{j,k}(x) = 2^{j/2} \, \psi \left(2^j x - k \right), \quad j, k \in \mathbb{Z}, \quad (4)$$

where j is the length-scale and k determines the spatial localization of the wavelet. Both j and k are integers when $x \in [0, 1]$. Hence we choose to normalize x by dividing it by the distance around the latitude circle d. These wavelets constituting this basis are orthonormal with respect to the inner product

$$\begin{aligned}
\langle \psi_{j,k}, \psi_{m,n} \rangle &= \int_0^d \psi_{j,k}(x) \, \psi_{m,n}(x) \, \mathrm{d}x \\
&= \begin{cases} 1, & j, k = m, n, \\ 0, & j, k \neq m, n. \end{cases}
\end{aligned} \quad (5)$$

Thus any function, $f(x)$, on the domain $[0, d]$ can be expanded in terms of the orthonormal basis as

$$f(x) = \sum_{j=0}^{\infty} \sum_{k=0}^{2^j} c_{j,k} \psi_{j,k}(x), \quad (6)$$

where the coefficients $c_{j,k}$ are given as

$$c_{j,k} = \langle f(x), \psi_{j,k}(x) \rangle = \int_0^d f(x) \, \psi_{j,k}(x) \, \mathrm{d}x. \quad (7)$$

The imposed orthogonality conditions require basis functions to be discrete wavelets, not continuous wavelets (Daubechies, 1992).

Unlike the Fourier basis, where the basis functions are unique, there exists a variety of wavelet basis functions. Those of the WDM are based on the assumptions in Equations (2) and (3) above, which only require them to be
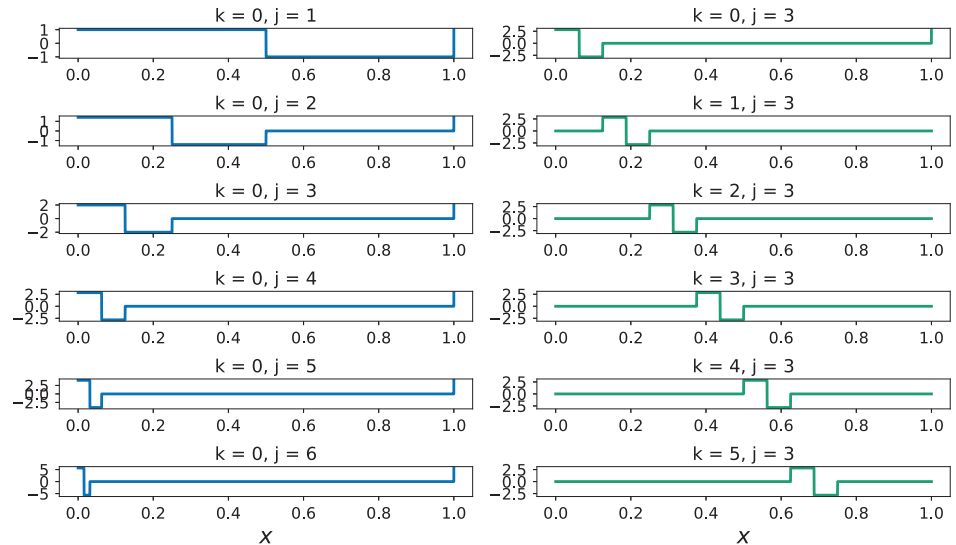
wavelets. The WDM used here is based on a Haar wavelet consisting of "box" functions (Figure 1).

Expressing the $v \, \mathrm{d}p/g$ and E fields in terms of a wavelet series yields

$$v \frac{\mathrm{d}p}{g} = \sum_{j'=0}^{\infty} \sum_{k'=0}^{2^{j'}} c_{j',k'}^{v} \, \psi_{j',k'}(x), \quad c_{j',k'}^{v} = \int_0^d v \frac{\mathrm{d}p}{g} \, \psi_{j',k'}(x) \, \mathrm{d}x \tag{8}$$

and

$$E = \sum_{j=0}^{\infty} \sum_{k=0}^{2^{j}} c_{j,k}^{E} \, \psi_{j,k}(x), \quad c_{j,k}^{E} = \int_0^d E \, \psi_{j,k}(x) \, \mathrm{d}x, \tag{9}$$

respectively. The zonally and vertically integrated meridional energy (ME) transport is given as

$$vE = \int_0^d \int_0^{p_s} Ev \frac{\mathrm{d}p}{g} \, \mathrm{d}x. \tag{10}$$

Inserting Equations (8) and (9) into Equation (10) and discretizing the vertical integral yields

$$vE = \sum_{l=0}^{L} \overline{vE_l} + \int_0^d \sum_{l=0}^{L} \left(\sum_{j=0}^{\infty} \sum_{k=0}^{2^j} c_{j,k}^{E,l} \, \psi_{j,k}^l(x) \right)$$
$$\times \left(\sum_{j'=0}^{\infty} \sum_{k'=0}^{2^{j'}} c_{j',k'}^{v,l} \, \psi_{j',k'}^l(x) \right) \mathrm{d}x, \tag{11}$$

where l denotes the height level in the dataset composed of L levels, and vE_l is the zonal-mean component of the energy transport at level l. When performing the zonal integral of Equation (11), only the terms with $j', k' = j, k$ will remain because of the orthogonality of the wavelets,

whereby

$$vE = \sum_{l=0}^{L} \left(\overline{vE_l} + \sum_{j=0}^{\infty} \left(\sum_{k=0}^{2^j} c_{j,k}^{E,l} \, c_{j,k}^{v,l} \right) \right) \tag{12}$$

is obtained. Note that the sum over k is truncated at $k = 2^j$, as higher values of k are localized outside the domain $[0, d]$.

The wavelet split in Equation (12) decomposes the ME transport into components based on length-scale and spatial localization of the systems transporting energy. The j-indices denote the length-scale of the systems, where a larger j denotes a smaller length-scale, and the k-indices denote the localization in the zonal direction. In Equation (12) the sums over l and j are interchangeable, whilst the sum over k is dependent on the sum over j. The expression can thus be rewritten as

$$vE = \overline{vE} + \sum_{j=0}^{\infty} vE_j, \tag{13}$$

where

$$vE_j = \sum_{l=0}^{L} \sum_{k=0}^{2^j} c_{j,k}^{E,l} \, c_{j,k}^{v,l}.$$

In the following the decomposition is performed on six scales, in addition to the meridional zonally symmetric flow. The first three scales correspond to length-scales greater than 3,400 km, and the last three to length-scales smaller than that threshold. Hence $j = 3$ and $j = 4$ are chosen as the separation between planetary and synoptic waves, since this is closest to the wavenumber 3–4 separation of the FDM. The Python implementation of the WDM applied for the computations in this project is available
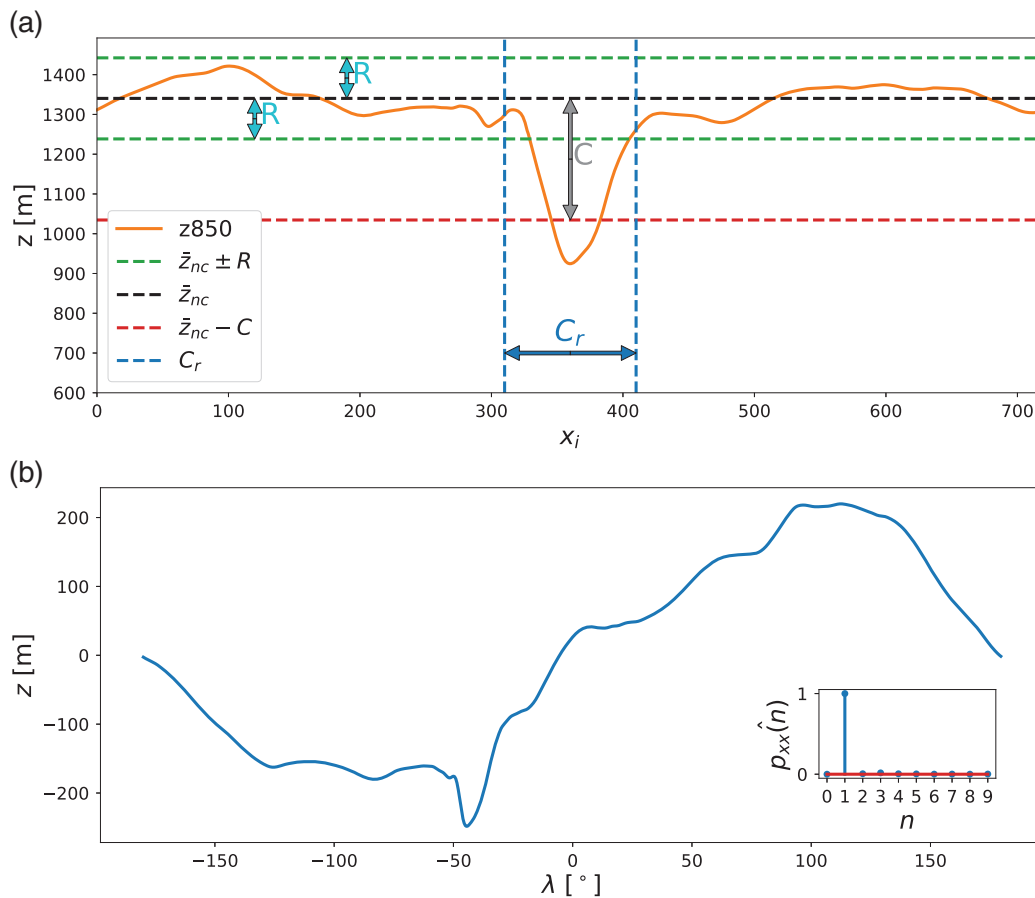
FIGURE 2 (a) is an illustrative example of the conditional filter applied on geopotential height at 850 hPa at 70°N. The shown $z850$ is one of fields marked as a cyclone by the filter, $\bar{z}_{nc}$ is the mean of the $z850$ field outside the cyclone region C_r, R is the maximum z-variation threshold limiting the variability outside C_r, and C is the minimum cyclone threshold defining the depth of the depression in $z850$ relative to $\bar{z}$. Here x_i denotes the indices of the data points of the rotated field. (b) is an illustrative example of the power spectrum-based filter used for retrieving the planetary waves. One example is shown (blue line) and the associated normalized power spectrum (inset plot) of this field

in a GitHub repository (https://github.com/tuohei/wdm; accessed 7 May 2020).

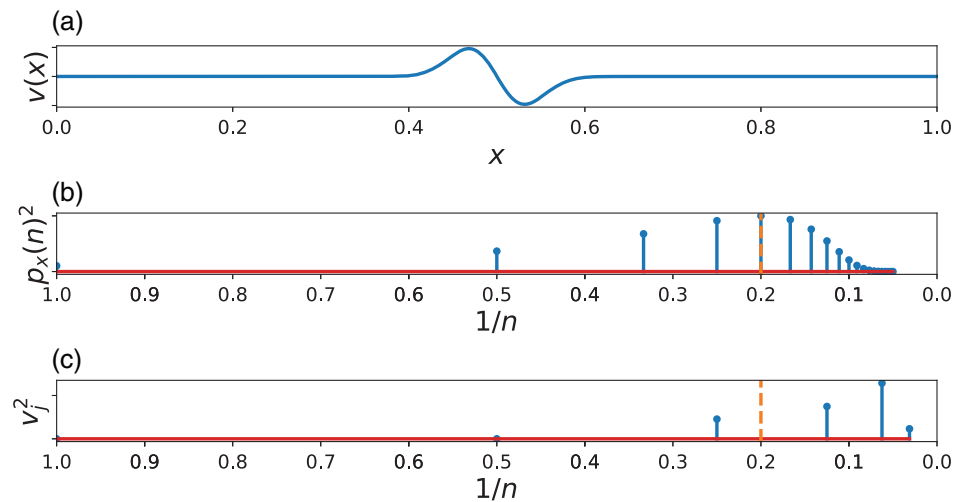## 2.4 | Cyclones and planetary waves in ERA-Interim

The present study applies the ERA-Interim reanalysis data (Dee *et al.*, 2011) produced by the European Centre for Medium-Range Weather Forecasts (ECMWF). The ERA-Interim reanalysis is used instead of the more state-of-the-art ERA5 reanalysis, since the analysis in GB16 is also based on ERA-Interim, and the main objective of the present study is to re-evaluate the findings based on the FDM presented in that study. Similarly to GB16, the atmospheric fields used in the energy transport are considered with a 0.5° latitude and longitude resolution, and at 60 vertical model levels, and with a 6 hr time resolution.

Time steps where the atmospheric state is characterized by single cyclones but show little influence

by planetary waves are found by applying a conditional filter on the 850 hPa geopotential height field ($z850$). The longitudinal cross-section of the $z850$ field of a single cyclone is characterized by a sharp negative peak which often resembles a Gaussian function. Constraining the variation of the $z850$ field outside the influence domain of the cyclone hampers the effects of planetary-scale waves, and the field left is thus dominated by the single cyclone.

The conditional filter is constructed by two thresholds: the cyclone threshold, C, providing the strength of the depression in the $z850$ field, and the variation threshold, R, limiting the planetary wave activity. The length-scale, C_r, is defining the cyclone region. This region is the region of influence of the isolated cyclone, defined as a distance of ~1,000 km at both sides of the maximum depression of the $z850$ field. The length of C_r is chosen such that it is well below the length-scale of synoptic systems at 70°N. The R indicates the upper limit for deviations in the $z850$ field outside C_r from the mean of the outside field (Figure 2).

FIGURE 3 (a) The longitudinal cross-section of the geostrophic winds of the synthetic (Gaussian) cyclone, and (b) is the power spectrum of the geostrophic winds in (a). (c) is the wavelet scale spectrum of the geostrophic winds in (a). The orange dashed line marks the approximate length-scale of the synthetic system. The x-axis of (b) and (c) are set to length-scale $1/n$ for simplicity of comparison, where n is the zonal wavenumber

3 │ RESULTS

3.1 │ Synthetic cyclones

First, as an illustrative example to show the basic concepts, the FDM and WDM are applied on synthetic data. Synthetic data are first generated using a Gaussian function, meant to represent the longitudinal geopotential height of a single cyclone (geostrophic winds in Figure 3a). The Gaussian is a localized function which ensures that no variability on the planetary scale is present in the synthetic data. Essentially the synthetic fields could represent any field, not just the geostrophic winds. These demonstrations are provided to show special cases where both the FDM and WDM may have problems attributing correctly the transport contributions to planetary- and synoptic-scale systems.

The power spectrum of the geostrophic winds associated with the synthetic cyclone (Figure 3b) reveals that approximately one third of the power of the wind field is found in the planetary range (wavenumbers 1–3 placed at the $1/n$-scale at approximately 0.5, 0.33, and 0.25 respectively). This does not correspond well with the length-scale of the synthetic cyclone, which is a clear

Planetary waves are found by imposing two conditions on the power spectrum of the $z850$ field. The power of wavenumber $n = 1$ is required to be greater than its climatological mean for the considered period, and additionally the power of the remaining wavenumbers is required to be less than 10% of the power of wave 1. This yields $z850$ fields which are predominantly dominated by a wave 1 pattern. Wave 1 is chosen as the criterion for planetary waves as it is on average found to be the most dominant wave type in the power spectrum of $z850$.

synoptic-scale system; the synthetic cyclone is localized, but has by construction, and what is evident by inspection by eye, a length-scale corresponding to approximately wavenumber 5.

The inaccurate representation by a Fourier decomposition of the synthetic cyclone is due to the localization of the system. This is demonstrated by the application of the WDM on the same geostrophic winds of the synthetic cyclone (Figure 3c). Note that the scale spectrum (Figure 3c) and the power spectrum (Figure 3b) are not directly comparable: the length-scales in the wavelet scale spectrum are decreasing at a higher rate than the length-scales in the power spectrum. Hence the number of j-scales presented is smaller than the number of Fourier wavenumbers n since each j-scale is composed of 2^{j-1} coefficients. For example, j-scale 4 consists of eight coefficients and corresponds to a length-scale of approximately 1,700 km at 70°N, whereas for the WDM wavenumber $n = 4$ corresponds to a length-scale of 3,400 km, given a distance around latitude 70° of ~13,700 km.

The wavelet decomposition (Figure 3c) appears to resolve these winds in the synthetic case better than does the Fourier decomposition (Figure 3b). With a separation at scales $j = 3$ and $j = 4$ between planetary and synoptic waves, the wavelet method results in a clear majority of power at synoptic scales, whilst the Fourier method yields an even distribution of power between planetary and synoptic scales when a split between wavenumber $n = 3$ and $n = 4$ is applied. Note again that wavenumber $n = 4$, the first wavenumber in the synoptic range, corresponds to a length-scale of approximately 2,200 km at 70°N, which is larger than the first synoptic j-scale ($j = 4$).

The wavelet method is known to be shift variant. The spread of power between the wavelet coefficients will be dependent on the spatial localization of the decomposed
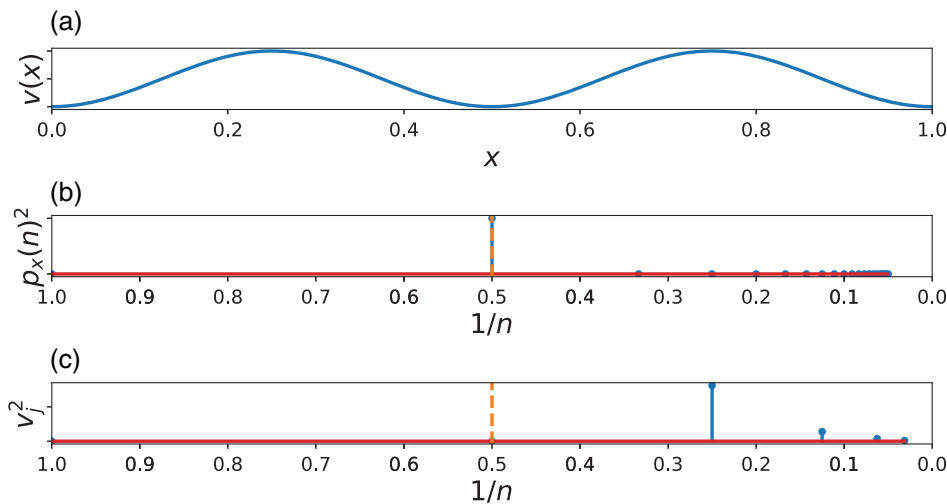
FIGURE 4 (a) Wave 2 structure. (b, c) are as in Figure 3, but for the wave 2 field in (a)

field. However the total power, sum over all coefficients, will remain constant, which is important for the usefulness of the wavelet method for decomposing the energy transport (Daubechies, 1992). This property, combined with the fact that planetary waves are not localized, may limit the accuracy of the wavelet method when it comes to the description of planetary-scale waves. This is demonstrated by applying both methods on a synthetic wave 2 structure.

The wave 2 (Figure 4a) is phase-shifted such that its projection onto the j-scale 2 is zero (Figure 4c), even though it length-scale-wise corresponds to the scale represented by $j = 2$. The sinusoidal wave 2 is a basis function of the Fourier decomposition. This, combined with the fact that the Fourier method is shift invariant, yields that the wave 2 structure will always fall on the corresponding coefficients independent of the spatial localization of the decomposed field, and thus resolves the wave 2 structure perfectly. This example demonstrates that for the WDM, power is shifted to higher scales when the large-scale waves are out of phase with respect to the wavelet basis.

These demonstrations with synthetic data show that the WDM represents localized systems better than the FDM in terms of a separation between planetary- and synoptic-scale contributions. However, since the WDM does not explicitly resolve all wavenumbers, there appears a misrepresentation of systems at the length-scales associated with these unrepresented wavenumbers. In addition, the WDM may have a spread of power from planetary non-localized systems to smaller scales, leading to an misrepresentation of these non-localized system. The spread of power will occur when the phase between the wavelets and the geophysical fields is such that the planetary-scale wavelets are out of phase with the planetary features of the geophysical fields. In comparison, the non-localized waves are well represented with the FDM, since the Fourier basis by nature is non-localized. The synthetic situations
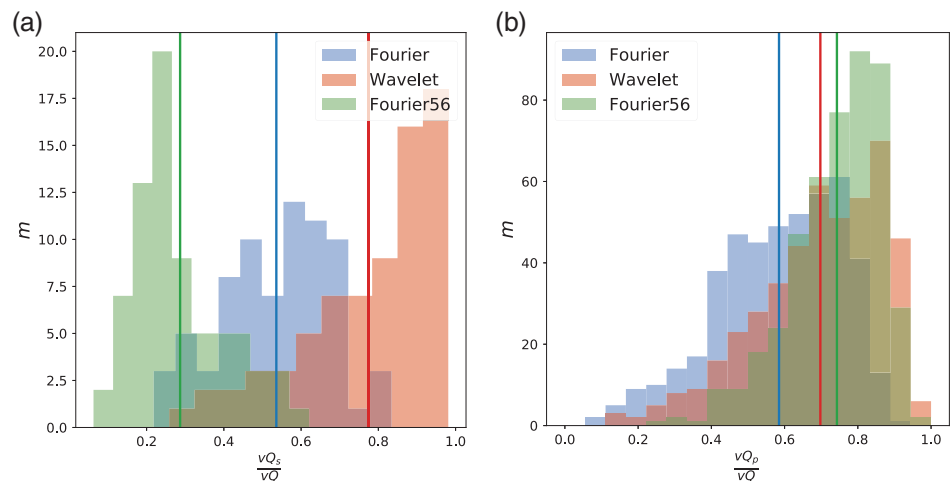
presented here are chosen to show extreme cases for both the FDM and WDM. Hence these are not representative for the general circulation in the atmosphere. These extreme cases are chosen to illustrate the plausible misrepresentations occurring in both methods. However this does not indicate that the WDM generally misrepresents the planetary-scale contribution, and the FDM the contributions by localized synoptic-scale systems.

Both the FDM and WDM are linear methods. This implies that a superpositioned field decomposed by these methods will be the superposition of the decompositions of the individual components of the field. Hence the misrepresentation which might be induced by extreme cases resembling the synthetic ones will be partly hidden in the mean.

3.2 | ERA-Interim cyclones and planetary waves

Should cases similar to the synthetic cyclone exist in the ERA-Interim data, the FDM will have trouble attributing the transport correctly in these situations. A conditional filter, as defined in Section 2.4, is therefore applied on ERA-Interim data in order to reveal such cases in real data. The filter is designed to extract cases with localized cyclones but weak planetary wave activity. Applying the conditional filter on ERA-Interim data, cases which resemble the idealized cyclone are found at 70°N. The filter is applied with several values of thresholds C and R (Figure 2). In total 73 such cases are identified by the conditional filter. For the extracted cases the FDM and WDM are then computed. The fraction of total energy transport in the synoptic range is plotted as a histogram in Figure 5a for the FDM with both a wavenumber separation between $n = 5$ and 6 (FDM56; as in GB16) and $n = 3$

and 4 (FDM34), as well as for the WDM with a separation at $j = 3$ and 4.

When applied on the filtered cases, the FDM56 attributes on average $\sim$30% of the transport to synoptic waves, whereas both the FDM34 attributes over 50% and the WDM over 75% to these waves (Figure 5a). Hence it is evident that the separation between planetary and synoptic waves between $n = 5$ and $n = 6$ does not capture well the characteristics of the isolated systems at 70°N. The FDM34 resolves the isolated systems better than does FDM56, since some of the planetary coefficients in FDM56 have been transferred to the synoptic range.

As a contrasting method to the filter to extract fields that are composed of isolated cyclones, fields characterized by strong planetary-scale waves are found through conditions imposed on the z850 power spectrum. Hence this method can be used to assess the capability of both the FDM and WDM to decompose planetary-scale transport correctly. The fields found by this method have no constraint on their phase, hence the fields may not necessarily correspond to problematic cases for the WDM, as for example that shown in Figure 4. Here the fractions of transport in the planetary range are computed similarly to those computed for the cases found by the conditional filter. In total 461 situations are identified where the wave 1 structure is the dominant pattern of the z850 (Figure 5b). For these cases FDM56 attributes on average $\sim$75% of the transport to the planetary scales. The WDM attributes $\sim$70% to the planetary scales, whilst FDM34 attributes $\sim$60% to these scales. For these cases a large fraction of transport in the planetary range is expected; the FDM56 provides on average the largest fraction with the WDM following closely.

The difference between the WDM and FDM34 is not as large as the difference between WDM and FDM56 for the synoptic cases, but it is evident that the WDM yields more average transport in the synoptic range than does the FDM34. For the planetary cases, the FDM56 yields the largest average fraction of the transport in the planetary range, whilst FDM34 yields the smallest fraction. Additionally FDM34 is closer to the WDM when considering both the synoptic and planetary cases found by the two fields. Hence for the rest of the study, the wavenumber separation between $n = 3$ and 4 will be used when referred to the FDM.

For the extreme filtered cases considered in Figure 5, the FDM and WDM attribute differently as regards the planetary and synoptic scales. However, in general the transport appears to be attributed similarly by the two methods. As an example, the time series for one winter season (DJF) is shown in Figure 6, where the planetary and synoptic components of both FDM and WDM are shown. The season shown is the 1985–1986 winter. This winter season has no special statistical characteristics; it is a typical winter season in terms of the attribution of transport to planetary scales, both by the FDM and WDM. Performing a linear regression of the planetary contribution of the FDM on the planetary contribution on the WDM yields $r^2 = 0.82$, which indicates that the two time series are strongly correlated. The mean r^2 for winter seasons is $\overline{r^2} = 0.83$. Hence the two methods are describing the planetary- and synoptic-scale transport contributions similarly in the winter season. There is some variation between the transports, which is to be expected since they are based on methods that are fundamentally different, however the large agreement of the transports
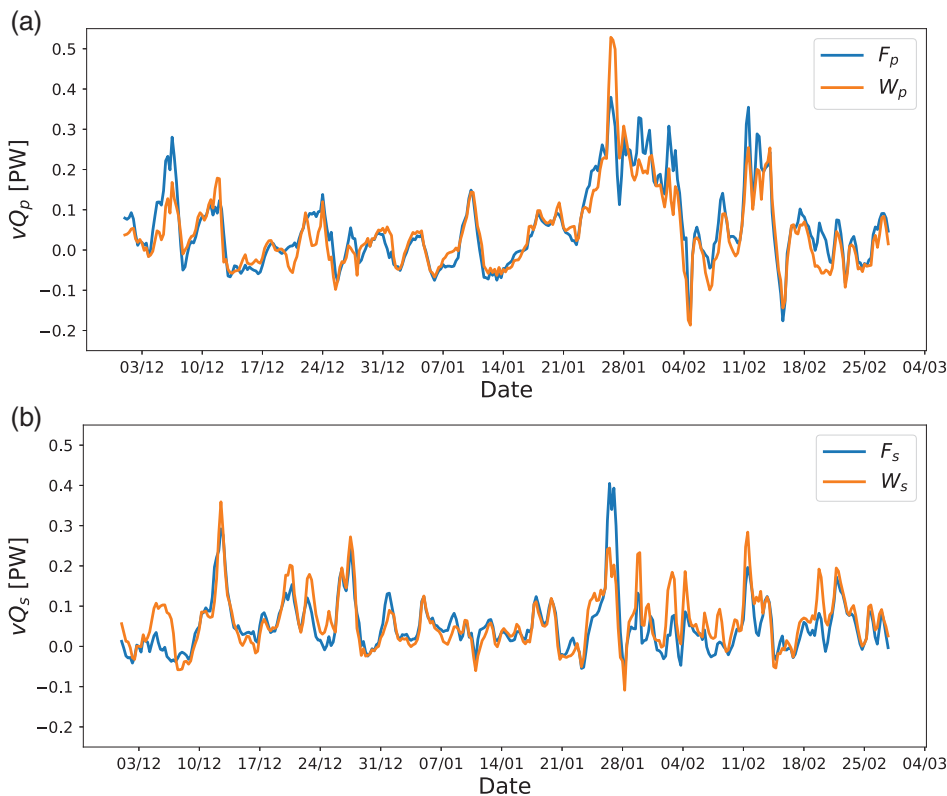
(a)

(b)

yields a strong argument for the existence of meaningful separation of transport by planetary- and synoptic-scale systems.

Next, FDM and WDM are applied on unfiltered data for latitudes $\phi \geq 60°N$ and averaged over time (Figure 7). The WDM with a separation of planetary and synoptic waves between scales $j = 3$ and $j = 4$ (Figure 7a) and the FDM with wavenumber separation at $n = 3$ and 4 (Figure 7) yield similar time-averaged latent heat transport for the studied period (1979–2017). The largest differences in the distribution between planetary and synoptic waves are found at low to mid latitudes (not shown), whilst in the high latitudes the differences are small. The fact that the independent methods yield similar time averages strengthens the credibility of both methods to represent the true distribution of transport between planetary- and synoptic-scale waves. But it does not guarantee that the methods actually solve individual time steps equally, as the time average only indicates the mean distribution between transport at planetary and synoptic scales. This difference in individual time steps is evident from the amount of described eddy-transport variance by both methods, presented in Table 1. The WDM yields higher amounts of described eddy-transport variance by both the planetary- and synoptic-scale transport. The transport components of the two methods are also regressed on each other, which shows that the planetary components describe approximately 70% of the variance in the other and the synoptic

component approximately 60% of the variance in the other. This indicate that there are differences between the methods although the time averages are similar. Although similar time-average transports are found using both methods, the difference in described variance may be a contributing factor to the differences in the regressions on Arctic temperatures. Localized systems are still resolved differently, as indicated in Figure 5, which affects the regressions on surface temperatures as shown in the following section.

3.3 | Regressions on Arctic temperatures

The relationship between the latent heat transport across 70°N and the mean 2 m temperature in the Arctic region (above 70°N) can be examined by using a linear regression analysis (e.g., Wu and Straus (2004); Graversen and Burtu (2016)). Here we compute lagged regressions per latitude based on the assumption that a correlation between anomalies in the zonal-mean atmospheric latent heat transport into the Arctic and consecutive anomalies in near-surface temperature inside the Arctic indicates the temperature response to the incoming flux of latent heat. Figure 8 shows the regression of mean 2 m temperature anomalies north of 30°N in response to transport anomalies across 70°N from the FDM and WDM, respectively. The regressions are based on daily data from the time period 1979–2017, at a spatial resolution of 2.5°. Time

FIGURE 7 Meridional latent heat transport and its components as a function of latitude. (a) Wavelet split into meridional circulation ($j = 0$), planetary waves ($j = 1$–3), and synoptic waves ($j = 4$–6). (b) Fourier split into meridional circulation ($n = 0$), planetary waves ($n = 1$–3), and synoptic waves ($n = 4$–20)
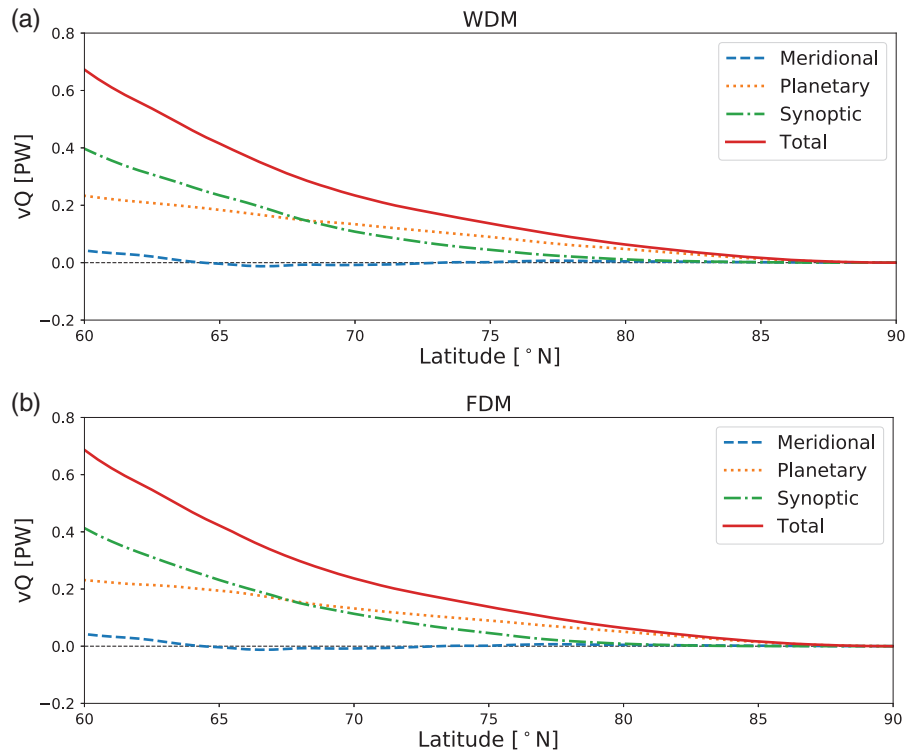
TABLE 1 r^2 coefficients from regressions of both the WDM and FDM total eddy transport on the planetary (p) and synoptic (s) components and from regressions between the components of the two methods

	FDMp	FDMs	Total
WDMp	0.73	0.04	0.64
WDMs	0.07	0.63	0.48
Total	0.60	0.42	1.00

lags up to 20 days are implemented to show the time frame of the temperature response to latent heat transport anomalies. The annual cycle is removed in both the transport data and the temperature data, and a 7-day running mean filter is applied. The black lines indicate areas in the time–latitude plane with statistically significant results based on a Monte-Carlo approach, in which the regression coefficients are compared to 5,000 regressions, where the phases are shifted randomly while keeping the power spectrum time series the same as the original one. A regression is considered statistically significant at the 99% (95%) level if less than 1% (5%) of the synthetic data yield more extreme values in an absolute sense than the original regression coefficient.

The regressions in Figure 8 based on the FDM, are as in GB16 but with a wavenumber separation of planetary and synoptic waves between wavenumbers 3

and 4 relative to the earlier work. This shift of separation yields a larger fraction of time-average transport in the synoptic range at 70°N which is closer to that indicated by the WDM. The FDM suggests that the latent heat transport of planetary waves (Figure 8a) contributes significantly to the subsequent warming of the Arctic. From the regressions on the transport split by the WDM (Figure 8c) it is found that the effect of the planetary wave transport on temperature is weaker than that obtained by the FDM. The weaker effect of planetary transport might be because of an under-representation of planetary waves in the WDM, combined with the fact that localized systems yield an enhanced planetary transport in the FDM.

Regressions of temperature on FDM synoptic transport (Figure 8b) can be intepreted in the light of the predominant enhanced temperature gradient which likely gives rise to increased baroclinic instability and to enhanced activity by synoptic systems: the regressions yield negative temperature anomalies north of 70°N and positive anomalies south of 70°N at the time of the anomaly, indicating an enhanced temperature gradient which sets up favourable conditions for baroclinic instability. The FDM regressions lack signals of warming by synoptic-scale waves in the Arctic. When instead performing the split with the WDM, the synoptic transport pattern shows positive temperature anomalies all over the Arctic for positive time lags (Figure 8d). The signal of an enhanced temperature gradient is present in the WDM regressions as
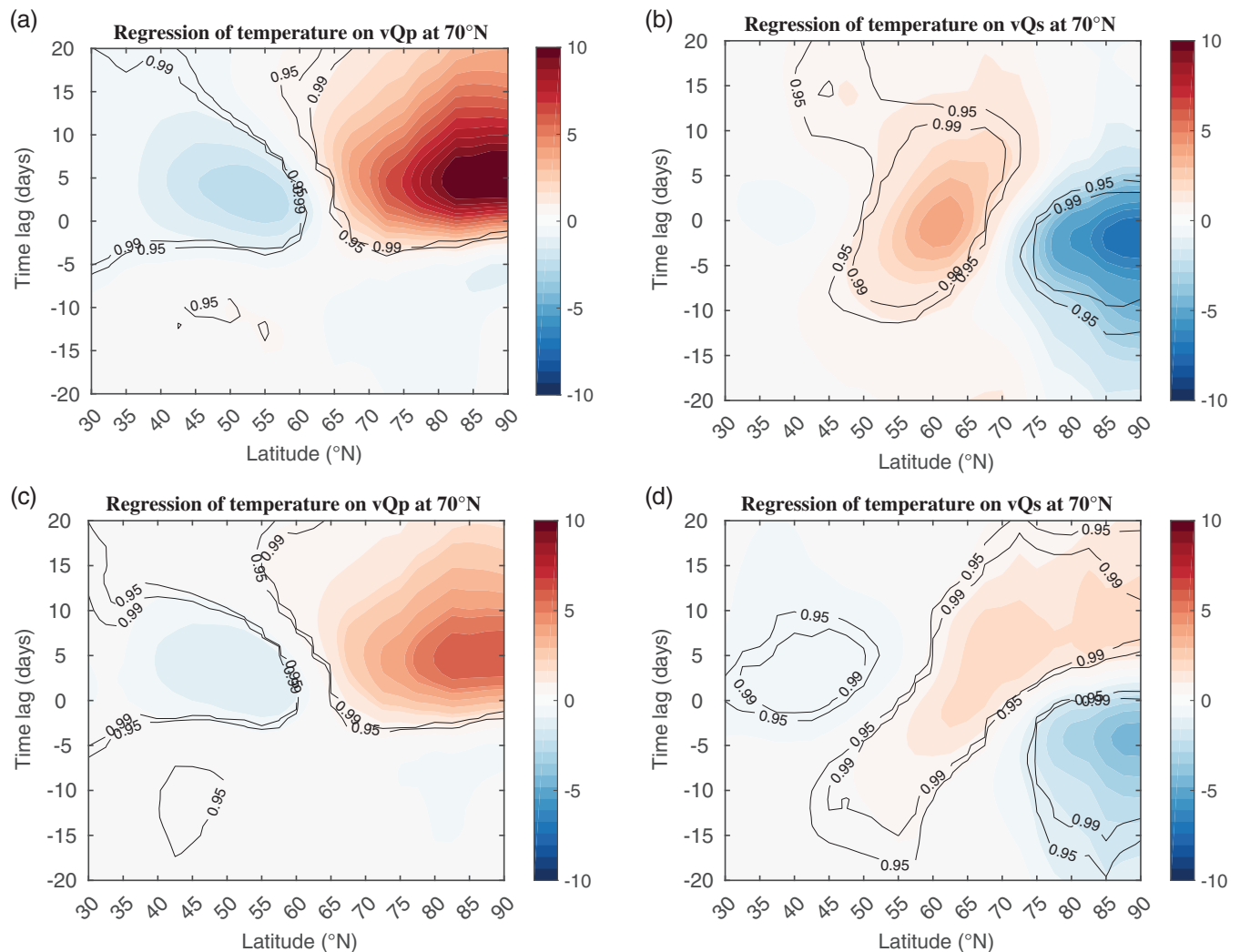
FIGURE 8 Regressions of temperature on (a) the planetary $n = 1 - 3$ and (b) synoptic $n = 4 - 20$ latent heat transport decomposed with the FDM, and (c) planetary $j = 1 - j = 3$ and (d) synoptic $j = 4 - j = 6$ decomposed with the WDM. The colours represent the regressions coefficients in K/PW, and the black contours denote the 0.95 and 0.99 significance levels found by a Monte-Carlo approach

well, but shifted towards negative timelags. This indicates again the presence of increased baroclinic instability associated with large synoptic-scale activity, but the signal of enhanced temperature gradient and Arctic cooling appears before the transport anomaly is at its maximum, in contrast to what is suggested by the FDM. Hence the enhanced baroclinic instability will contribute to the formation of the synoptic-scale systems which transport the energy into the Arctic, to the extent that the Arctic shows positive temperature regressions at positive timelags.

In summary, the difference between the FDM and WDM is especially noticeable for the synoptic part of the transport. From the filtered cases, the FDM is found to represent synoptic systems less accurately than does the WDM, and one effect is shown in the difference between the FDM and WDM synoptic regressions. From

the FDM there is no clear evidence of warming in the Arctic due to the synoptic latent heat transport at 70°N, whereas the regressions on the WDM synoptic transport show an Arctic warming approximately 10 days after the transport anomaly at 70°N. This implies that, according to the WDM, synoptic systems contribute significantly to the subsequent warming of the Arctic, which is in agreement with other previous studies (Woods and Caballero, 2016; Boisvert et al., 2016; Messori et al., 2018).

4 | DISCUSSION AND CONCLUSIONS

Fourier series are widely used to decompose atmospheric fields into processes acting on different scales

(Peixoto and Oort, 1992). The present study highlights the problem of using non-localized basis functions to decompose atmospheric fields. Investigations of synthetic fields and filtered ERA-Interim data demonstrate that the FDM has difficulties attributing the latent heat transport of individual cyclones. This is a fundamental problem of the Fourier series expansion of spiked signals (e.g., Smith 2007). The WDM circumvents this problem by building upon basis functions localized both in space and scale. Hence the split into synoptic and planetary waves in the presence of localized systems appears more appropriate to be represented with the WDM than FDM.

The problem with localized systems is not present in the classical split into stationary and transient eddies (Peixoto and Oort, 1992). However this split is fundamentally different, as it is based on a time-filtering and does not impose any conditions on the spatial scales of the systems; both synoptic- and planetary-scale systems can be stationary or transient. The length-scale split, based on either the FDM or WDM, does not regard the time-scales at which atmospheric systems occur. The length-scale-based methods are used to separate systems based on the dynamical processes leading to their formation. Planetary-scale systems are often forced by orography and land–sea contrasts, whilst the synoptic-scale systems are usually formed by instability processes in the atmosphere. These instabilities are more frequent in some regions (e.g., in the North Atlantic), hence the synoptic-scale systems are not only transient systems but do also have a stationary part. Due to orography and land–sea contrast, the planetary waves too have a stationary component, but these waves are also travelling inducing a transient component. Hence the classical split into stationary and transient eddies is unable to separate between the planetary- and synoptic-scale systems, which is accomplished by the FDM and WDM.

From the inspections of the synthetic cases, the WDM appears as an attractive alternative to the FDM. Also based on isolated systems in ERA-Interim data, it is reasonable to assume that the WDM performs better than the FDM for this type of system. In particular, comparisons of the FDM and WDM for cases found with the conditional filter (Figure 5a) suggests that the WDM outperforms the FDM when it comes to the representation of strongly localized systems.

The WDM resolves synoptic localized systems with little spread of power to planetary scales. However the WDM has some caveats: the wavelet series expansion is shift variant, that is, the wavelet coefficients are dependent on the localization of the atmospheric fields relative to the wavelets. The shift variance affects the planetary waves the most since there are few coefficients representing these

length-scales as compared to the coefficients representing the synoptic scales. In addition, the planetary-scale waves are not localized, which makes the wavelet basis less suitable to attribute these waves. However the WDM has been tested for several different shifts (not shown here), and the results do not change significantly. In addition, the WDM does not attribute the transport into all wavelengths, as demonstrated by the Haar basis (Figure 1). This implies that some of the wavelengths will be represented by different scales than those of these waves. The WDM will also have a dependency on the chosen wavelet, since the values of the wavelet coefficients are dependent on the shape of the wavelet (Daubechies, 1992; Domingues *et al.*, 2005). The WDM in this study is based on the Haar wavelet, which is a box function. It is unlikely to find patterns similar to the Haar wavelet in the atmosphere. However, other discrete wavelet families (Daubechies, 1992) are often not significantly closer to atmospheric states, and are often difficult to relate directly to the length-scales of systems. Thus the Haar wavelet, although its shape is somewhat artificial, serves the purpose of this study as the alternatives are not obviously better.

In GB16 the wavenumber separation between planetary and synoptic waves was chosen between $n = 5$ and $n = 6$. At 70°N wavenumber $n = 5$ represents a length-scale of ~ 2700 km. This is smaller than the threshold of synoptic scales, which is defined as $\sim 4,000$ km (Holton and Hakim, 2013). Shifting the wavenumber separation to between $n = 3$ and $n = 4$ results in more similar decompositions for the FDM and the WDM. The separation of planetary and synoptic waves between $n = 3$ and $n = 4$ is also physically more accurate with respect to the length-scale separation of synoptic and planetary waves at 70°N (Holton and Hakim, 2013). Thus the threshold scale at which the planetary and synoptic scales are separated is not completely arbitrary, and careful consideration of the latitudinal dependence of the length-scale of waves when choosing the threshold is recommended for future studies.

Regressions of temperature on WDM synoptic transport show a positive correlation in the Arctic with a timelag of approximately 10 days (Figure 8d), implying a warming of the Arctic following enhanced energy transport. In contrast, the FDM synoptic transport (Figure 8b) shows no significant warming signal at these latitudes. The fact that the latent heat transport by synoptic systems results in an Arctic warming is consistent with previous studies (Woods *et al.*, 2013; Woods and Caballero, 2016; Messori *et al.*, 2018). It appears as a clear weakness of the FDM that the Arctic warming by synoptic waves is not well captured. Both the warming due to the WDM and FDM planetary latent heat transport show a similar pattern, but the signal is weaker for the WDM case. This weaker signal is

likely due to a misrepresentation of some of the planetary waves by the WDM and the fact that localized systems, likely misrepresented by the FDM, are more correctly represented by the WDM. The truth likely lies somewhere between the results of the WDM and FDM, since the WDM under-represents planetary-scale waves whilst the FDM over-represents these scales. However the importance of latent heat transport by planetary-scale waves is indicated both by the WDM and FDM and the warming effect is stronger than for the synoptic-scale waves, in agreement with GB16.

In summary, spatially localized systems are poorly represented by sine functions, hence a Fourier series approach will misrepresent these systems and should be used with care. The FDM captures the main effect of planetary latent heat transport on Arctic temperatures, but thus fails to accurately represent the synoptic transport effect. The WDM captures the overall effect of planetary as well as the synoptic latent heat transport on Arctic temperatures. A test of the robustness of the WDM results is to perform a similar analysis as in the present study based on a different wavelet basis. The WDM and FDM show a similar effect of planetary latent heat transport on Arctic temperatures. Hence planetary waves play an important role on Arctic temperatures, as uncovered in GB16, and the FDM seems to adequately represent the latent heat transport of planetary-scale systems. In general the FDM will over (under)represent and the WDM under (over)represent planetary (synoptic) transport. Thus it is likely that the true effect of planetary and synoptic transports lies somewhere between the WDM and FDM representations. Hence, when investigating effects of energy transport in the atmosphere at different scales, the FDM and WDM should be used together to form a more complete picture.

ORCID

Tuomas Heiskanen ![ORCID] https://orcid.org/0000-0003-0113-0627

REFERENCES

Boisvert, L.N., Petty, A.A. and Stroeve, J.C. (2016) The impact of the extreme winter 2015/16 Arctic cyclone on the Barents–Kara Seas. *Monthly Weather Review*, 144(11), 4279–4287. https://doi.org/10.1175/MWR-D-16-0234.1

Daubechies, I. (1992) *Ten Lectures on Wavelets*. Society for Industrial and Applied Mathematics, Philadelphia, PA.

Dee, D.P., Uppala, S.M., Simmons, A.J., Berrisford, P., Poli, P., Kobayashi, S., Andrae, U., Balmaseda, M.A., Balsamo, G., Bauer, P., Bechtold, P., Beljaars, A.C.M., van de Berg, L., Bidlot, J., Bormann, N., Delsol, C., Dragani, R., Fuentes, M., Geer, A.J., Haimberger, L., Healy, S.B., Hersbach, H., Hólm, E.V., Isaksen, L., Kållberg, P., Köhler, M., Matricardi, M., McNally, A.P., Monge-Sanz, B.M., Morcrette, J.-J., Park, B.-K., Peubey, C., de Rosnay, P., Tavolato, C., Thépaut, J.-N. and Vitart, F. (2011) The ERA-Interim reanalysis: configuration and performance of the data assimilation system. *Quarterly Journal of the Royal Meteorological Society*, 137, 553–597. https://doi.org/10.1002/qj.828

Domingues, M.O., Mendes, O. and da Costa, A.M. (2005) On wavelet techniques in atmospheric sciences. *Advances in Space Research*, 35(5), 831–842. https://doi.org/10.1016/j.asr.2005.02.097

Graversen, R.G. and Burtu, M. (2016) Arctic amplification enhanced by latent energy transport of atmospheric planetary waves. *Quarterly Journal of the Royal Meteorological Society*, 142, 2046–2054. https://doi.org/10.1002/qj.2802

Holton, J.R. and Hakim, G.J. (2013) *An Introduction to Dynamic Meteorology* (5th ed.) Academic Press, Cambridge, MA.

Koenigk, T., Brodeau, L., Graversen, R.G., Karlsson, J., Svensson, G., Tjernström, M., Willén, U. and Wyser, K. (2013) Arctic climate change in 21st century CMIP5 simulations with EC-Earth. *Climate Dynamics*, 40(11), 2719–2743. https://doi.org/10.1007/s00382-012-1505-y

Messori, G., Woods, C. and Caballero, R. (2018) On the drivers of wintertime temperature extremes in the high Arctic. *Journal of Climate*, 31(4), 1597–1618. https://doi.org/10.1175/JCLI-D-17-0386.1

Naakka, T., Nygård, T., Vihma, T., Sedlar, J. and Graversen, R. (2019) Atmospheric moisture transport between mid-latitudes and the Arctic: Regional, seasonal and vertical distributions. *International Journal of Climatology*, 39(6), 2862–2879. https://doi.org/10.1002/joc.5988

Peixoto, J.P. and Oort, A.H. (1992) *Physics of Climate*. American Institue of Physics, New York, NY.

Smith, J.O. (2007) *Mathematics of the Discrete Fourier Transform (DFT)* (2nd ed.) Available at: http://ccrma.stanford.edu/<spi-Sineqdollar>~<spi-Scineqdollar>jos/mdft/; accessed 7 May 2020.

Trenberth, K.E. and Caron, J.M. (2001) Estimates of meridional atmosphere and ocean heat transports. *Journal of Climate*, 14(16), 3433–3443. https://doi.org/10.1175/1520-0442(2001)014<3433:EOMAAO>2.0.CO;2

Vallis, G.K. (2017) *Atmospheric and Oceanic Fluid Dynamics: Fundamentals and Large-scale Circulation* (2nd ed.) Cambridge University Press, Cambridge, UK.

Woods, C. and Caballero, R. (2016) The role of moist intrusions in winter Arctic warming and sea ice decline. *Journal of Climate*, 29(12), 4473–4485. https://doi.org/10.1175/JCLI-D-15-0773.1

Woods, C., Caballero, R. and Svensson, G. (2013) Large-scale circulation associated with moisture intrusions into the Arctic during

winter. *Geophysical Research Letters*, 40(17), 4717–4721. https://doi.org/10.1002/grl.50912

Wu, Q. and Straus, D.M. (2004) AO, COWL, and observed climate trends. *Journal of Climate*, 17(11), 2139–2156. https://doi.org/10.1175/1520-0442(2004)017<2139:ACAOCT>2.0.CO;2

Yoshimori, M., Abe-Ouchi, A. and Laîné, A. (Nov 2017) The role of atmospheric heat transport and regional feedbacks in the Arctic warming at equilibrium. *Climate Dynamics*, 49(9), 3457–3472. https://doi.org/10.1007/s00382-017-3523-2